JCTC Journal of Chemical Theory and Computation

Article

pubs.acs.org/JCTC

Excited-State Gradients in Polarizable QM/MM Models: An Induced Dipole Formulation

Maximilian F. S. J. Menger,[†,‡] Stefano Caprasecca,[†] and Benedetta Mennucci*[,†]

[†]Dipartimento di Chimica e Chimica Industriale, University of Pisa, Via G. Moruzzi 13, 56124 Pisa, Italy

[‡]Institut für Theoretische Chemie, Universität Wien, Währinger Strasse 17, A-1090 Wien, Austria

Supporting Information

ABSTRACT: Charge and structural relaxation of electronically excited states in embedded systems are strongly affected by the environment. It is known that the largest part of environment effects comes from electrostatics. However, polarization can also play a role by tuning the electronic and geometrical properties of the states, finally modifying the fluorescence. Here we present the formulation of analytical excited-state gradients within a polarizable QM/MM approach and their implementation within the ONIOM framework. A time-dependent DFT level of theory is used in combination with an induced dipole formulation of the polarizable embedding. The formation and relaxation of the bright excited state of an organic dye (DAPI) intercalated in a DNA pocket is used to quantify the role played by the mutual polarization between the QM subsystem and the embedding and also to investigate the onset of overpolarization, which is a known limit of the model with potentially detrimental effects. On the one hand, the results indicate the robustness of the QM-classical interface and, on the other hand, show the non-negligible effect of polarization between DAPI and a DNA pocket in determining the fluorescence properties of the embedded dye.

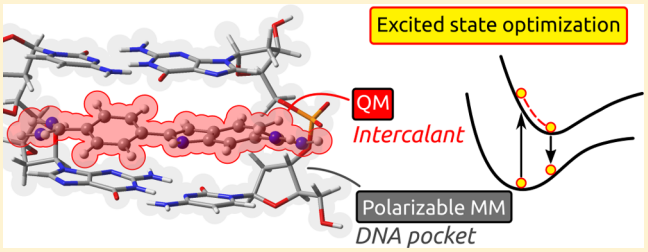

1. INTRODUCTION

The theoretical investigation of photoinduced processes in molecular systems requires a proper description of excited-state properties and structures. Accurate wave function based *ab initio* methods, such as coupled cluster or complete active space self-consistent field approaches, are computationally very demanding and therefore still unfeasible for large systems. The computational limitations become even more evident when the same molecular systems are embedded in an environment. Even if the latter can largely affect the properties of the electronic states and their energy ordering, possibly modifying the mechanisms of the light-driven process, its *ab initio* description cannot be achieved. In those cases, an effective strategy is to introduce multiscale models, which combine a selected QM level of theory with a classical model for the environment. A good compromise in accuracy and computational cost for the QM level is provided by time-dependent density functional theory (TDDFT), whereas both continuum and atomistic approaches have been developed to introduce environment effects at a classical level. In QM/continuum methods the environment is approximated as a structureless medium described through its macroscopic dielectric properties,[1−3] whereas in QM/atomistic approaches molecular mechanics (MM) force fields are generally employed.[4−6]

Many different implementations exist within hybrid QM/classical methods for describing electronic excitation processes.[7,8] In the case of MM descriptions, the most common one is to use an electrostatic embedding where the excitation of the QM subsystem happens in the presence of a set of fixed charges which represent the environment atoms. Within this approach, the theoretical and computational formalism is exactly the same as that used for the isolated molecular system, since the external fixed charges can be included in the calculations as additional "nuclei," and their effects on the QM system are through one-electron operators equivalent to those used for describing nuclei-electrons interactions. This means that also the extension of the model to excited-state derivatives with respect to both geometrical and nongeometrical parameters is straightforward, as it does not require any additional environment-specific term.

When a polarizable embedding is used, instead, the presence of an environment response, which depends on the QM charge density, introduces new specificities in both the theoretical formulation and the computational implementation. Within TDDFT, the most common way to proceed, known as linear response (LR) formulation, is to introduce an effective response of the environment to a transition density. Such a formulation is consistent with linear response theories, and it can be easily generalized to excited-state analytical gradients. This extension has been already presented for QM/continuum models[9,10] and for the Effective Fragment Potential (EFP)[11] formulation of QM/atomistic models.[12] It has been shown[13−16] that the LR formulation lacks the capability of describing the

Received: May 8, 2017
Published: July 12, 2017

DOI: 10.1021/acs.jctc.7b00475
J. Chem. Theory Comput. 2017, 13, 3778−3786

relaxation of the environment response with the excited-state density. To overcome this shortcoming, various models have been introduced that add a state-specific (SS) correction to the transition energies using either continuum[17−19] or atomistic[20,21] descriptions of the environment response. Such corrections have also been extended to analytical and numerical derivatives for continuum models[10,22,23] showing that the effects on excited-state geometries are generally limited even if the contribution to the energy is not negligible. As a matter of fact, we have to note that the SS energy correction for a relaxed excited state can be large for continuum models where the whole response is entirely determined by the charge density of the selected state. On the contrary, for polarizable MM, the SS contribution refers only to the polarizable part of the response, while the purely electrostatic term is represented by fixed charges. One can thus expect that for polarizable QM/MM the SS effect on geometries will be even smaller than that observed for continuum models.

In this work, we extend our own implementation of a polarizable QM/MM model based on induced dipoles[24,25] (from now on MMPol), which we have been developing in the last years, to allow for the calculation of excited-state gradients, through an analytical formulation. The implementation makes use of the ONIOM framework[26] to account for all non-electrostatic contributions to the forces.

The formulation is applied to the study of the absorption and fluorescence of an organic dye intercalated in DNA. The comparison of the newly implemented approach with a standard QM/MM based on electrostatic embedding shows that the inclusion of mutual polarization between the QM subsystem and the embedding (here a model of a DNA pocket) leads to significant differences in the excited-state geometries. These differences are finally reflected in the change of fluorescence upon intercalation. A study of absorption and emission energies with increasing basis set size is also carried out to probe the range of applicability of the model, particularly for what concerns the problem of overpolarization.

2. THEORY

2.1. Polarizable QM/MM: Induced Dipole Formulation. In this article a polarizable version of QM/MM is used, where the classical atoms carry isotropic polarizabilities in addition to the fixed charges commonly used in standard nonpolarizable approaches. Within this formalism, the QM−MM interaction energy displays an additional term, namely the interaction energy between the induced dipoles μ_k at the classical atoms k and the QM region. As a result, the Fock or Kohn−Sham operator can be written, within a self-consistent field (SCF) approach such as Hartree−Fock (HF) or DFT, as

$$F_{pq} = h_{pq} + \sum_i [\langle pi|qi\rangle - c_x\langle pq|ii\rangle] + f^{xc}_{pq} + V^{es}_{pq} + V^{pol}_{pq} \tag{1}$$

Here the scaling parameter c_x is introduced to interpolate between pure DFT ($c_x = 0$) and HF ($c_x = 1, f^{xc} = 0$). The matrix elements of the DFT exchange-correlation functional are denoted as f^{xc}_{pq}, and the two-electron coulomb integrals $\langle pi|qi\rangle$ are given in the Dirac notation. Throughout this paper we will use the common notation, whereby occupied molecular orbitals (MOs) are labeled i, j, ..., virtual orbitals are labeled a, b, ..., and generic orbitals are labeled p, q, ... Greek letters (μ, ν,...) are used as indices for atomic orbitals.

The two terms V^{es}_{pq} and V^{pol}_{pq} in eq 1 represent the matrix elements of the MMPol (or induced dipoles) operators, which correspond to the electrostatic and polarization interaction energies. While V^{es}_{pq} is a pure one-electron contribution expressed as the product of the MM charges and the electrostatic potential integrals, the second term depends on the QM charge density, through the induced dipoles on the N_{pol} polarizable classical atoms. The dipoles are obtained by solving a set of coupled linear equations yielding the following linear problem

$$\mathbf{T}\boldsymbol{\mu}^{ind} = \mathbf{E} \tag{2}$$

where $\mathbf{E}$ is the electric field generated on the polarizable MM atoms by the QM region and the MM charges, and the $N_{pol} \times N_{pol}$ matrix $\mathbf{T}$ is

$$\mathbf{T} = \begin{pmatrix} \boldsymbol{\alpha}_1^{-1} & \mathcal{T}_{1,2} & \dots & \mathcal{T}_{1,N_{pol}} \\ \mathcal{T}_{2,1} & \boldsymbol{\alpha}_2^{-1} & \dots & \mathcal{T}_{2,N_{pol}} \\ \vdots & \vdots & \ddots & \vdots \\ \mathcal{T}_{N_{pol},1} & \mathcal{T}_{N_{pol},2} & \dots & \boldsymbol{\alpha}_{N_{pol}}^{-1} \end{pmatrix} \tag{3}$$

In the last equation the diagonal elements are the inverse of the atomic polarizability tensors, while $\mathcal{T}_{ij}$ are the (damped) dipole interaction tensors:

$$\mathcal{T}^{\alpha\beta}_{ij} = -\frac{\delta_{\alpha\beta}}{|\vec{r}_i - \vec{r}_j|^3}\lambda_3 + 3\frac{|\vec{r}_i - \vec{r}_j|^\alpha |\vec{r}_i - \vec{r}_j|^\beta}{|\vec{r}_i - \vec{r}_j|^5}\lambda_5 \tag{4}$$

The damping factors λ_3 and λ_5 are introduced to avoid the well-known *polarization catastrophe* and are functions of the interatomic distance.[27−30]

The presence of the induced dipoles makes the MMPol interaction term dependent on the QM system, which itself contributes to the electric field that induces the MMPol dipoles. This mutual interaction problem is automatically solved within the standard SCF iterative strategy.

2.2. Polarizable QM/MM: Linear Response Formalism. Once the hybrid QM/MMPol method is implemented for the ground-state approaches (DFT, HF), it is straightforward to extend the scheme to linear response excited-state methods, namely TDDFT, TDHF, and CIS. Applying the Casida formulation, the working equations one has to deal with are of the type[31]

$$\boldsymbol{\Lambda}|\mathbf{X}, \mathbf{Y}\rangle = \boldsymbol{\Omega}\boldsymbol{\Delta}|\mathbf{X}, \mathbf{Y}\rangle \tag{5}$$

where

$$\boldsymbol{\Lambda} = \begin{pmatrix} \mathbf{A} & \mathbf{B} \\ \mathbf{B}^* & \mathbf{A}^* \end{pmatrix}, \quad \boldsymbol{\Delta} = \begin{pmatrix} \mathbf{1} & \mathbf{0} \\ \mathbf{0} & -\mathbf{1} \end{pmatrix} \tag{6}$$

$\mathbf{A}$ and $\mathbf{B}$ represent the rotation matrices that couple the occupied and virtual blocks of orbitals. $(\mathbf{X} + \mathbf{Y})_n$ is the transition vector of the n-th electronic eigenstate of the system, with corresponding excitation energy Ω_n. Within the QM/MMpol formalism, the $\mathbf{A}$ and $\mathbf{B}$ matrices explicitly include an environment term:

$$A_{ai,bj} = \delta_{ab}\delta_{ij}(\varepsilon_a - \varepsilon_i) + \langle ij|ab\rangle + f^{xc}_{aibj} + \mathcal{V}^{MMPol}_{iajb} - c_x\langle ia|jb\rangle \tag{7}$$

$$B_{ai,bj} = \langle ij|ab\rangle + f^{xc}_{aibj} + \mathcal{V}^{MMPol}_{iajb} - c_x\langle ia|bj\rangle \tag{8}$$

DOI: 10.1021/acs.jctc.7b00475
J. Chem. Theory Comput. 2017, 13, 3778−3786

Here ε_p is the SCF energy of orbital p, f^{xc}_{aibj} is the linear response of the exchange correlation functional, and $\mathcal{V}^{MMPol}_{iajb}$ represents the MMPol response term. This is only dependent on the dipoles, as the charges are constant and their derivatives vanish as a consequence:

$$\mathcal{V}^{MMPol}_{iajb} = -\sum_k \boldsymbol{\mu}^{ind}_k[\varphi_j\varphi_b^*]\cdot\int d\mathbf{r}\varphi_i(\mathbf{r})\varphi_a^*(\mathbf{r})\frac{(\mathbf{r}_k-\mathbf{r})}{|\mathbf{r}_k-\mathbf{r}|^3} \tag{9}$$

The integral term represents the electric field due to the transition density $\varphi_i(\mathbf{r})\varphi_a^*(\mathbf{r})$ computed at the MM atom k, while $\boldsymbol{\mu}^{ind}_k[\varphi_j\varphi_b^*]$ is the induced dipole due to the transition density $\varphi_j(\mathbf{r})\varphi_b^*(\mathbf{r})$.

2.3. Analytic Gradients of the Excited States. The expressions for the energy derivative of a QM system represented by its wave function Ψ and the corresponding Hamiltonian H with respect to a generic parameter λ can in general be written as

$$E^\lambda = \langle\Psi|\frac{\partial H}{\partial\lambda}|\Psi\rangle + 2\left\langle\frac{\partial\Psi}{\partial\lambda}\middle|H|\Psi\right\rangle \tag{10}$$

The first term is the so-called Hellmann−Feynman force, while the second term (the wave function response to the perturbation) is the Pulay force.[32] With the help of the chain rule, one can show that for fully variational energy functionals the Pulay force vanishes and only the Hellmann−Feynman term remains. This would also be desirable for the LR-TDDFT equations above, which are however nonvariational energy functionals. Furche et al.[33] remedied this by starting directly with a constructed, fully variational Lagrangian $\mathbf{L}$, having the same stationary points and forces as the nonvariational TDDFT energy functional $\mathbf{G}$:

$$\mathbf{G}[\mathbf{X},\mathbf{Y},\boldsymbol{\Omega}] = \langle\mathbf{X},\mathbf{Y}|\boldsymbol{\Lambda}|\mathbf{X},\mathbf{Y}\rangle - \boldsymbol{\Omega}(\langle\mathbf{X},\mathbf{Y}|\boldsymbol{\Delta}|\mathbf{X},\mathbf{Y}\rangle) \tag{11}$$

This approach was later generalized by Scalmani et al.[9] for continuum solvation models and by Carmineo et al.^(A) for a MM polarizable embedding described by fluctuating charges.[34] In this article we also follow this approach and choose an analogous fully variational Lagrangian $\mathbf{L}[\mathbf{X},\mathbf{Y},\boldsymbol{\Omega},\mathbf{Z},\mathbf{W}]$ for MMPol:

$$\mathbf{L} = \mathbf{G}[\mathbf{X},\mathbf{Y},\boldsymbol{\Omega}] + \sum_{ia} Z_{ia}F_{ia} + \sum_{pq,p\le q} W_{pq}(S_{pq}-\delta_{pq}) \tag{12}$$

Here F_{pq} are matrix elements of the Fock operator containing the MMPol terms (see (1)), S_{pq} are elements of the MO overlap matrix, and $\mathbf{Z}$ and $\mathbf{W}$ are Lagrangian multipliers. Evaluation of the stationary points of $\mathbf{L}$ with respect to the excitation energy and excitation vectors leads to the normalization condition for the excitation vectors $\mathbf{X}$, $\mathbf{Y}$ and the LR-TDDFT equations. The newly introduced Lagrangian multipliers, namely the Z-vector $\mathbf{Z}$ and the energy-weighted density $\mathbf{W}$, ensure that the Kohn−Sham (or Hartree−Fock) equation is satisfied and that the MOs are orthonormal.[33] The price for avoiding the calculation of the perturbed MOs is that now $\mathbf{Z}$ and $\mathbf{W}$ need to be computed. The working equations to do this follow directly from the stationary condition of $\mathbf{L}$ with respect to the MO coefficients. Thanks to the symmetry of $\mathbf{W}$ one can derive equations for the occupied-virtual block that are only depending on $\mathbf{Z}$, the so-called Z-vector equations:[35]

$$\sum_{jb}(A+B)_{ia,jb}Z_{jb} = C1_{ai} - C2_{ai} + G^+_{ai}[P^\Delta_{kl}] + G^+_{ai}[P^\Delta_{bc}] \tag{13}$$

In these equations we use the same notation as in Scalmani et al.,[9] with the unrelaxed difference density as the occupied-occupied and virtual−virtual block of P^Δ and Z_{ia} for the occupied-virtual block, to indicate its origin in the Lagrangian multiplier Z, namely

$$P^\Delta_{ij} = -\frac{1}{2}\sum_a[(X+Y)_{ia}(X+Y)_{ja} + (X-Y)_{ia}(X-Y)_{ja}] \tag{14}$$

$$P^\Delta_{ab} = +\frac{1}{2}\sum_i[(X+Y)_{ia}(X+Y)_{ib} + (X-Y)_{ia}(X-Y)_{ib}] \tag{15}$$

$$Z_{ia} = P^\Delta_{ia} \tag{16}$$

The expressions of $G^\pm_{ai}$ and $C1_{ai}$ and $C2_{ai}$ can be found in ref 9.

After $\mathbf{Z}$ is computed, the energy-weighted density can be obtained as a function of $\mathbf{Z}$. Once all Lagrangian multipliers have been evaluated, one can write down the analytic gradient of $\mathbf{L}$, as

$$\Omega^\xi = \mathbf{L}^\xi = \frac{1}{2}\sum_{iajb}[(A+B)^\xi_{iajb}(X+Y)_{ia}(X+Y)_{jb} + (A-B)^\xi_{iajb}(X-Y)_{ia}(X-Y)_{jb}] + \sum_{ia}Z_{ia}F^\xi_{ia} + \sum_{pq,p\le q}W_{pq}S^\xi_{pq} \tag{17}$$

Here we use again the short term notation, where the superscript ξ indicates a derivative with respect to a generic nuclear coordinate. This expression can be written in more compact form, by using an atomic orbitals basis instead of the MO basis used so far

$$\Omega^\xi = \sum_{\mu\nu}h^\xi_{\mu\nu}P^\Delta_{\mu\nu} + \sum_{\mu\nu}S^\xi_{\mu\nu}W_{\mu\nu} + \sum_{\mu\nu\kappa\lambda}\langle\mu\nu|\kappa\lambda\rangle^\xi\Gamma_{\mu\nu\kappa\lambda} + \omega^{xc,\xi} + \omega^{MMPol,\xi} \tag{18}$$

where $\Gamma_{\mu\nu\kappa\lambda}$ is the two-particle density matrix; its expression can be found in ref 33. Formally, this equation differs from the analytic gradient expression of an isolated system only for the last term. However, the environment also affects all the densities. The explicit MMPol term in eq 18 can be divided into two parts:

$$\omega^{MMPol,\xi} = \sum_{\mu\nu}V^{MMPol,\xi}_{\mu\nu}P^\Delta_{\mu\nu} + \sum_{\mu\nu\kappa\lambda}\mathcal{V}^{MMPol,\xi}_{\mu\nu\kappa\lambda}(X+Y)_{\mu\nu}(X+Y)_{\kappa\lambda} \tag{19}$$

Eq 20 involves only atomic basis function derivatives in the case when only derivatives with respect to QM coordinates are considered. The first term depends on the change in the one-particle density matrix upon excitation and involves the ground-state matrix elements of the MMPol operator

$$\sum_{\mu\nu}V^{MMPol,\xi}_{\mu\nu}P^\Delta_{\mu\nu} = \sum_k\boldsymbol{\mu}^{ind}_k\mathbf{E}^{\Delta,\xi}_k + \sum_{k,l}[\mathbf{E}^\Delta_k\mathbf{T}^{-1}_{kl}\mathbf{E}^\xi_l] + \sum_{k,l}[\mathbf{E}^\Delta_k(\mathbf{T}^{-1}_{kl})^\xi\mathbf{E}_l] \tag{20}$$

where $\mathbf{E}^\Delta_k$ is the change in the electronic field at the classical atom k corresponding to the change in the one-particle density matrix. The MMPol matrix $\mathbf{T}$ is only dependent on coordinates

DOI: 10.1021/acs.jctc.7b00475
J. Chem. Theory Comput. 2017, 13, 3778−3786

of the MM atom, and its derivative vanishes in the case of a differentiation with respect to QM coordinates. The second term in eq 20 arises from the derivative of the $(\mathbf{A} + \mathbf{B})$ matrix and is therefore specific of linear response theory, namely

$$\sum_{\mu\nu\kappa\lambda} \mathcal{V}^{\mathrm{MMPol},\xi}_{\mu\nu\kappa\lambda}(X+Y)_{\mu\nu}(X+Y)_{\kappa\lambda} = 2\sum_{k,l} \boldsymbol{E}_k^{(X+Y),\xi}\boldsymbol{T}^{-1}_{kl}\boldsymbol{E}_l^{(X+Y)} + \sum_{k,l} \boldsymbol{E}_k^{(X+Y)}\boldsymbol{T}^{-1,\xi}_{kl}\boldsymbol{E}_l^{(X+Y)} \tag{21}$$

where

$$\boldsymbol{E}_k^{(X+Y),\xi} = \sum_{\mu\nu} (X+Y)_{\mu\nu}\boldsymbol{E}^{\xi}_{k,\mu\nu} \tag{22}$$

$$\boldsymbol{E}_l^{(X+Y)} = \sum_{\mu\nu} (X+Y)_{\mu\nu}\boldsymbol{E}_{l,\mu\nu} \tag{23}$$

Eq 18 can be finally summed to the standard DFT contribution to give the expression for the total energy gradient of each state n in the presence of a polarizable embedding:

$$E_n^{\xi} = E^{\xi}_{\mathrm{GS}} + \Omega_n^{\xi} \tag{24}$$

The description of the ground-state DFT gradient contribution E^{ξ}_{GS} is presented in the original paper on the formulation of analytical energy gradients within the QM/MMPol scheme.[25]

The implementation of the analytical derivatives for excited-state TDDFT/MMPol has been performed in a locally modified version of Gaussian.[36] Such implementation makes use of the ONIOM scheme.[26] The advantage of the implementation within the ONIOM scheme relies on the fact that all nonelectrostatic contributions to the forces (bonded and nonbonded ones) are available, and the additional force terms generated by the presence of the electrostatic and polarization interactions can be added independently.

3. A TEST CASE

As a test case, we compared the polarizable embedding scheme presented in the previous section with a standard electrostatic embedding in determining the structural and spectroscopic properties of the doubly protonated fluorescent stain 4′,6-diamidino-2-phenylindole (here referred to as DAPI, shown in Figure 1a) intercalated in DNA. DAPI is a common fluorescent marker for DNA with important applications as an antiparasitic, antibiotic, antiviral, and anticancer drug.[37] It is known to interact with DNA in a nonunivocal manner, both by intercalation and minor groove binding, and to specifically change its photophysical properties according to the different environments. In this test study we will focus on the intercalation, and we will consider the pocket formed by two pairs of cytosine and guanine (CG) DNA bases connected by the sugar skeleton. This choice has been based on the fact that intercalation was proposed for GC-rich DNA.[38,39] The interaction of DAPI with poly[d(G-C)$_2$] results in large visible spectral shifts and enhanced fluorescence.

The total system considered, including DAPI and the DNA fragment, is neutral: the DAPI molecule has a net charge of +2, while the partial charges on the DNA sum to −2. We also note that the intercalated DAPI is located with its positively charged amidine groups close to the phosphate backbones and indole H(N) oriented toward the major groove (see Figure 1b).

Ground-state (GS) and excited-state (ES) geometry optimizations were performed for both the free and the intercalated DAPI; in the latter case both the polarizable and the electrostatic embedding schemes have been used. The excited state of interest is the lowest singlet state of the DAPI molecule, characterized by a HOMO−LUMO transition (see Figure 2). For the ES calculations two levels of theory were employed: CIS and TDDFT within the Tamm-Dancoff approximation (TDA) using CAM-B3LYP and M06-2X functionals. For the intercalated system the definition and the structure of the DNA pocket was taken from ref 40 and kept frozen during the optimization of the DAPI. In the QM/MM calculations the standard AMBER parameters were used, as included in the Gaussian program suite,[36] for both electrostatic and nonelectrostatic contributions. In the QM/MMPol calculations, the isotropic atomic polarizabilities of Wang et al.[41,42] were employed, and the corresponding charges were

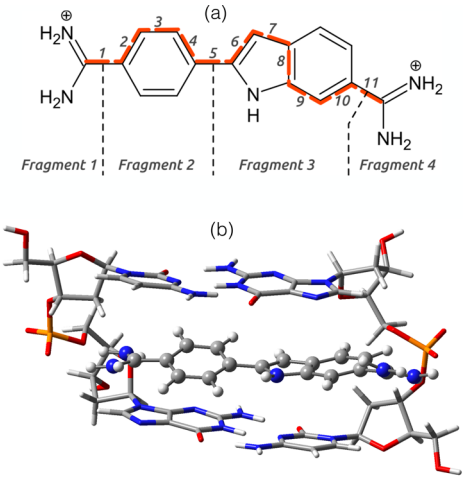

Figure 1. (a) Structure of DAPI. The dashed red line shows the bonds chosen to compute the bond length alternation (BLA) parameter. The dashed black lines define the fragments used in the charge distribution analysis. (b) Geometry of the DAPI intercalated within two GC DNA base pairs. The dotted lines are used to define the fragments of the DAPI chosen to carry out the charge analysis.

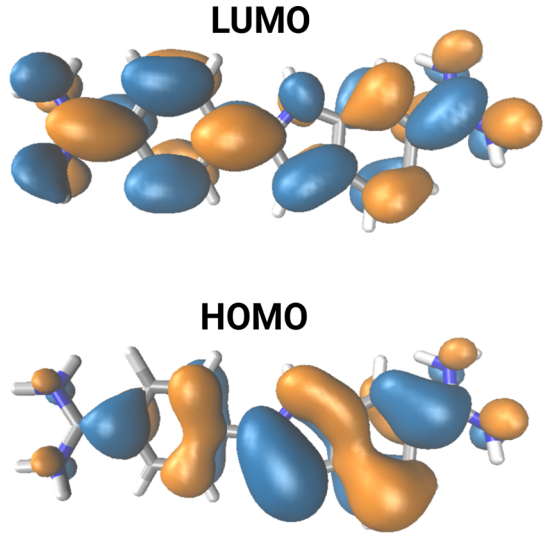

Figure 2. Isovalue surfaces of the orbitals contributing mainly to the state of interest.

DOI: 10.1021/acs.jctc.7b00475
J. Chem. Theory Comput. 2017, 13, 3778−3786

obtained by fitting the electrostatic potential including the induced dipoles, using our own PolChat tool.[43]

3.1. Structures and Charge Distributions. To assess the changes induced by intercalation on ground- and excited-state geometries of DAPI, 11 internal C−C bonds (marked in red in Figure 1) were chosen. From these bonds it is possible to define the bond length alternation (BLA), computed as the difference of the average single- and double-bond lengths. The BLA is often used as a measure of conjugation. Figure 3 shows

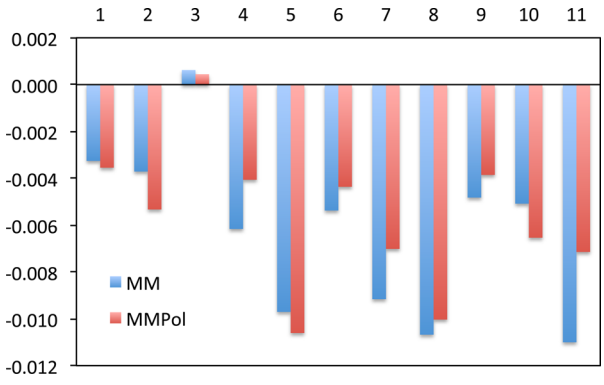

Figure 3. Variation of the selected bond lengths (Å) for the ground-state DAPI upon intercalation, using QM/MM and QM/MMPol models. All values are relative to those of the optimized free DAPI. All data are obtained at the CAM-B3LYP/6-31G(d) level. The numbering of the bonds is reported in Figure 1a.

the variation of the 11 selected bond lengths upon intercalation of the ground-state DAPI: the structures optimized at QM/MM and QM/MMPol levels are compared with those optimized for the free molecule.

Both QM/MM and QM/MMPol models predict a shortening of all the bonds considered (however limited to 0.012 Å at most), with the exception of bond 3. The BLA value is therefore unaffected (see Table 1). This indicates that, for the

Table 1. BLA (Å) and Dihedral Angle between the Benzene and Indole Fragments (δ, degrees), As Obtained from the Ground- and Excited-State Geometry Optimizations of the Free and the Intercalated DAPI[a]

	free	MM	MMPol
BLA(GS)	0.0328	0.0328	0.0336
BLA(EX)	−0.0049	0.0004	−0.0061
δ(GS)	29	21	15
δ(EX)	12	15	9

[a]In the latter case, both QM/MM and QM/MMPol results are reported.

present system, the effect of the intercalation on the ground-state bond lengths is very small, and no significant differences are introduced with the inclusion of a polarizable embedding.

A larger sensitivity to the environment is instead apparent in the central dihedral angle between the benzene and indole fragments. The cage effect of the DNA pocket is in fact expected to restrain the rotational degrees of freedom: indeed moving from the free molecule to the intercalated one a clear planarization is observed, which is more pronounced with the polarizable embedding (see Table 1).

The optimization of the excited state of interest, characterized by a strong HOMO−LUMO transition, was also carried out, employing the same embedding schemes as for the ground state. Figure 4 shows the differences in bond lengths for the excited-state optimized structure within the DNA pocket, compared to those of the free DAPI.

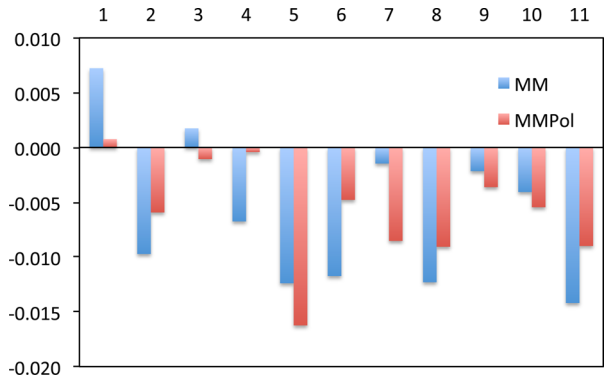

Figure 4. Variation of the selected 11 bond lengths (Å) for the excited-state DAPI upon intercalation, using QM/MM and QM/MMPol models. All values are relative to those of the optimized free DAPI. All data are obtained at the TDA-CAM-B3LYP/6-31G(d) level. The numbering of the bonds is reported in Figure 1a.

As observed for the ground state, also in the excited state the intercalation leads to a general shortening of the bonds (with the exception of bonds 1 and 3), but this time the differences are larger. The effect of the inclusion of the polarization is also more evident here than it was in the ground state. Indeed, not negligible differences between polarizable and nonpolarizable embeddings appear, for instance in the external bond 1 and the internal bonds 4−7. The BLA reflects these differences, as an increase with respect to the free geometry is predicted in QM/MM, oppositely to QM/MMPol (see Table 1). Moreover, the excited-state optimizations lead to a planarization for both the free and the intercalated DAPI (see Table 1), which is largest in the polarizable embedding.

The change in the conjugation path upon excitation is summarized in Figure 5. It is evident from the alternating pattern of the first eight bond lengths that the single (double) bonds tend to become shorter (longer), with a consequent increase in conjugation. This is confirmed by the lower BLA

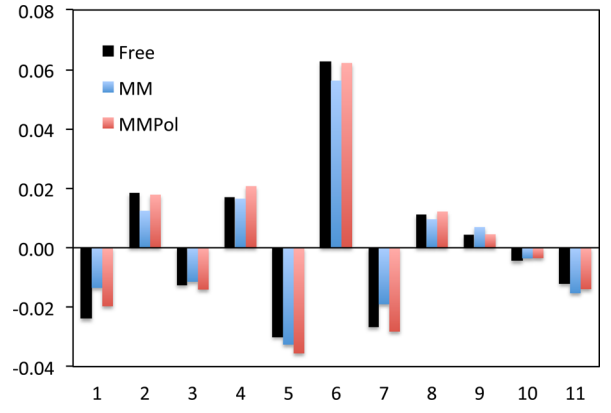

Figure 5. Difference between ground- and excited-state structures for the free and the intercalated DAPI. In the latter case both electrostatic (MM) and polarizable embeddings (MMPol) are shown. All data are obtained at the CAM-B3LYP/6-31G(d) level. The numbering of the bonds is reported in Figure 1a.

DOI: 10.1021/acs.jctc.7b00475
J. Chem. Theory Comput. 2017, 13, 3778−3786

values in the excited state and in the consistently more planar structures as shown in Table 1. We also remark that the bond length variation predicted with the polarizable embedding is larger than within the nonpolarizable QM/MM.

To better understand the structural rearrangement upon excitation, we also analyzed the charge redistribution by partitioning the DAPI into four different fragments and carrying out a Mulliken charge analysis both at ground- and excited-state optimized structures. The fragments considered are the two protonated amidine moieties (fragments 1 and 4), the benzene ring (fragment 2), and the indole fragment (fragment 3) (see Figure 1). The results obtained at the (TDA)CAM-B3LYP/6-31G(d) level are reported in Figure 6

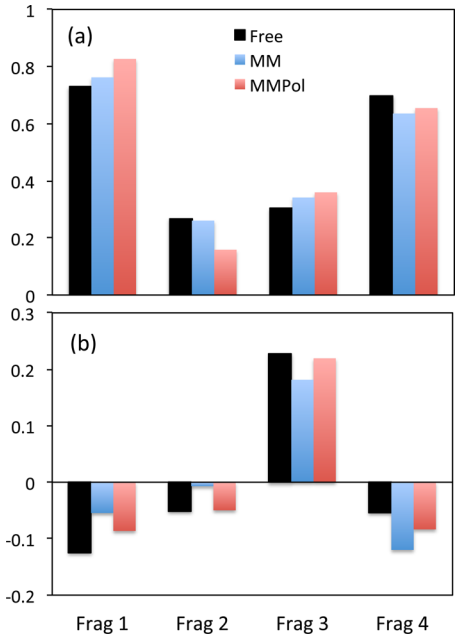

Figure 6. (a) Ground-state charge distribution (in au) localized on the four fragments as obtained for the free molecule and the intercalated one with the electrostatic and the polarizable embedding. (b) Differences between fragment charges in the excited and ground state. In all cases the geometries are those obtained for the selected electronic state and the selected model. The numbering of the fragments is reported in Figure 1a.

(data for the other functional and CIS are reported in the Supporting Information). In the free molecule in its ground state, the positive charge is mainly localized on the external amidine groups (1 and 4) as expected, and this distribution is only slightly affected by the intercalation.

Upon excitation, a significant redistribution of the density within the DAPI is observed: the (negative) charge moves from the indole to the external groups, reducing the charge difference between them. This charge-transfer picture is significantly reduced when the system is intercalated within a nonpolarizable embedding (MM), while it remains almost unchanged if the embedding can polarize (MMPol). This is indeed an interesting difference that is related to the structural differences induced upon excitation for both the free and the intercalated DAPI.

The atomistic nature of our model also allows a detailed analysis of the role played by each single component of the environment. To do that we have analyzed the interaction energies of DAPI with the four DNA moieties separately: cytosine (C) and guanine (G) bases, phosphate groups (P), and sugars (S). Their effect have been partitioned into a ground-state interaction term (between the MMPol distributions and the DAPI ground-state density) and the two response terms to the electronic excitation, namely the term entering in the TDDFT matrices (term 1) and the state-specific correction (term 2). The results are reported in Table 2. We first observe

Table 2. QM/MMPol Interaction Energies (kcal/mol) between DAPI and Selected DNA Moieties[a]

	ground state		excitation	
	total	Pol	term 1	term 2
C	−52.1	−1.8	−0.5	−0.1
G	−87.9	−2.8	−1.0	−0.2
P	−298.4	−2.2	−0.2	−0.0
S	207.9	−0.2	−0.5	−0.1

[a]The geometry is the QM/MMPol excited-state optimized one. The ground-state contribution due only to polarization is shown in brackets.

that the phosphate groups play a major role in stabilizing the ground-state energy: this is expected considering their high negative net charge. The DNA base pairs also contribute to stabilize the intercalated system, while the effect of sugar fragments is repulsive. When we move to the two terms which determine the response to the transition, a similar behavior is found: the effect of the phosphate groups almost disappears and that of guanine contributes twice with respect to cytosine bases (which is equivalent to sugars). These effects, when summed up, are those which determine the large difference found in the fluorescence shift for MM and MMPol. This simple analysis clearly shows that the response of the environment to the electronic transition behaves very differently from pure electrostatics.

3.2. Absorption and Fluorescence Energies. The optimized structures of ground and excited states allowed us to calculate and compare absorption and fluorescence emission energies of free and intercalated DAPI.

For QM/MMPol, the transition energies have been corrected so to account for the state-specific relaxation of the response of the embedding using the same formalism presented in refs 20 and 21. Note that such state-specific correction is only applied to the energies and not to the calculation of the gradients. While this is of little importance in the present study, as the effect is small (see Tables S7 and S8 in the Supporting Information), a state-specific formulation of MMPol is available, and we are currently working on implementing it in the gradients.

In this analysis, we also explore the impact of the choice of basis set. This was done, on the one hand, to inspect the convergence of the results to the infinite basis limit and, on the other hand, to probe the range of applicability of the polarizable QM/MM model, particularly for what concerns the detrimental effects of a possible overpolarization. Within the MM atoms, an effective remedy to overpolarization is included through the Thole scaling functions for the dipole−dipole interactions (which is also used in our implementation). What however remains is the possibility of the QM and MMPol subsystems to overpolarize. This is an intrinsic flaw of the model approximation and cannot be eliminated all together, although damping schemes have been proposed to mitigate the problem.[44,45] By increasing the size of the basis set, particularly including diffuse functions, one artificially increases the

DOI: 10.1021/acs.jctc.7b00475
J. Chem. Theory Comput. 2017, 13, 3778−3786

interaction range between QM and classical moieties, therefore becoming prone to overpolarization.

In Figure 7 the absorption and fluorescence energies are presented for a collection of basis sets, ranging from the

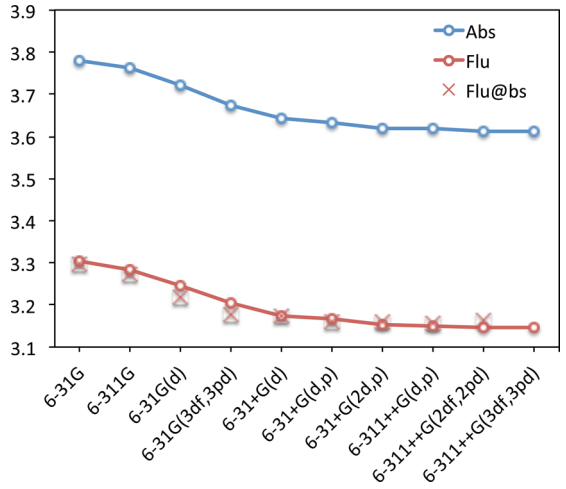

Figure 7. Absorption and fluorescence energies (in eV) for QM/MMPol with CAM-B3LYP and different basis sets. The QM/MMPol (CAM-B3LYP/6-31G(d)) ground-state optimized structure was used for the absorption, and the corresponding excited-state optimized structure was used for the fluorescence. The crosses correspond to the fluorescence energy calculated at the excited-state structure optimized using each selected basis set. All data have been obtained including the state-specific correction.

double-ζ 6-31G to a triple-ζ with diffuse and polarizable functions, 6-311++G(3df,3pd). The absorption and emission energies were computed using the same structure optimized at the ground or excited state at the CAM-B3LYP/6-31G(d) level. The red line, instead, refers to the emission energies where the excited-state geometries were optimized with each different basis set.

The results show that, for this system, overpolarization does not seem to be an issue, neither for single-point calculations nor for geometry optimizations. The absorption and emission excitation energies behave regularly with increasing basis set size, and no strong increase of the QM-MM interaction energy is observed. We also note that an increase in the number of core basis functions has a limited influence on the excitation energy, while additional polarizable or diffuse functions in the valence have a large effect (for instance compare results for 6-311G and 6-31G(3df,3pd)). This is an expected result, as an accurate description of the core electrons results in a better overall energy of the system, but excitations are mainly dependent on valence orbitals. We also tested the Dunning basis sets, where overpolarization occurred only for the augmented quadruple-ζ basis set (aug-cc-pVQZ). We also note that the effect of the basis set on the geometry is rather limited if a basis set including polarization functions is used (see the comparison of the two sets of fluorescence data).

The same basis set analysis has been repeated for the free and the QM/MM intercalated DAPI. The results are summarized in Figure 8 where we report the shift in both absorption and emission energies due to the intercalation as obtained with the polarizable and the electrostatic embedding.

The data reported shows that in both models the intercalation leads to a red shift of absorption and fluorescence.

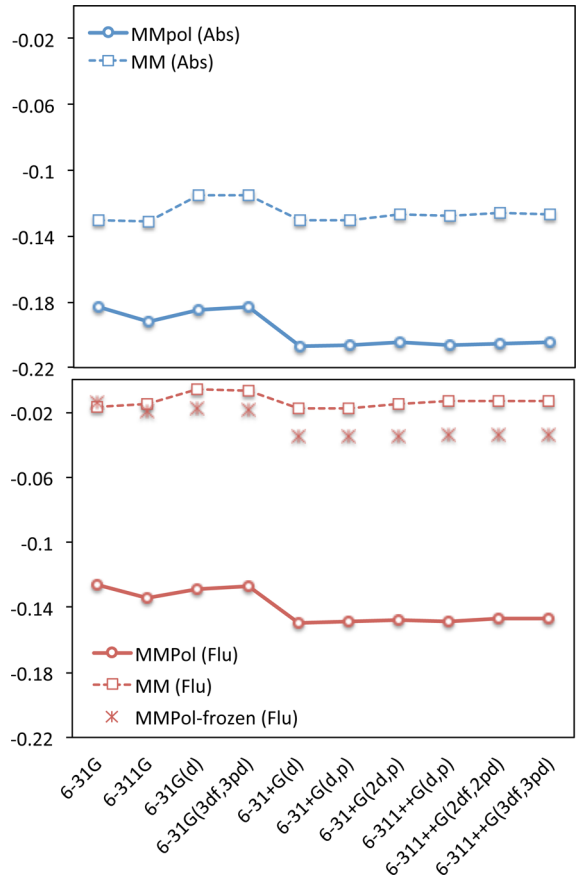

Figure 8. Shift of absorption (upper graph) and fluorescence energies (lower graph), in eV, upon intercalation, using QM/MMPol and QM/MM approaches with TDA/CAM-B3LYP and different basis sets. The MMPol-Frozen data refer to a model where any MMPol response to the excitation is switched off, as detailed in the text. In all calculations the ground- and excited-state geometries are those optimized at the QM/MM(Pol) level using (TDA)CAM-B3LYP/6-31G(d).

Moreover, the effect of the basis set is rather limited, and it becomes negligible if at least one diffuse and one polarization function are used. When comparing the electrostatic and the polarizable embedding schemes, it appears that the sensitivity to the basis set is more evident in the latter.

The most relevant result, however, is the red shift observed in the emission (ca. 0.1 eV) when the polarizable embedding scheme is used, compared to the electrostatic one. On the other hand, the differences in the shifts for the absorption energies are almost negligible (between 0.05 and 0.07 eV). At this stage, the comparison with experiments is extremely difficult as a much more extensive analysis of the system, in particular including a correct sampling of the DNA structure and of the solvent configuration, should be done. This kind of analysis is beyond the scope of the paper; however, we can note that the inclusion of polarization tends to increase the Stokes shift from 0.41 to 0.47 eV, which is somewhat closer to the experimental value of 0.68 eV.

We also note that the MMPol description leads to a general increase of the transition dipole moment at the excited-state geometry with respect to the free DAPI (data reported in Table S10 of the SI). The increase is of the order of 4−5%, while the QM/MM description gives a decrease of the order of 2−3%. To better understand the origin of these differences we have computed another set of data, obtained by switching off any

DOI: 10.1021/acs.jctc.7b00475
J. Chem. Theory Comput. 2017, 13, 3778−3786

MMPol response to the transition. Namely, we have neglected the $V_{ia,jb}^{MMPol}$ term of eq 9 from the TDDFT matrices. These data are reported in Figure 8, labeled "MMPol−frozen". It is interesting to note that for small basis sets the MMPol−frozen and MM values are very similar, but they start to diverge as soon as the basis set becomes flexible enough.

All these results indicate that the polarizable embedding has a larger effect in the excited than in the ground state and that using a nonresponsive embedding could prevent a complete relaxation of the excited state.

4. SUMMARY

We have presented the formulation and the implementation of the excited-state analytical gradients within a polarizable TDDFT/MM model based on induced dipoles. The theoretical formulation has been based on a variational formulation of the TDDFT approach, and the implementation has been carried out within the ONIOM formulation available in the Gaussian suite of codes. As a test case we have presented the application to the absorption and fluorescence properties of a well-known fluorescent marker for DNA, DAPI, intercalated in a GC-pocket. Despite its simplicity, this test has provided interesting results. First, the direct comparison between the electrostatic and the polarizable embeddings has shown that non-negligible effects due to the environment polarization are evident in the excited-state geometries and, as a result, in the emission energies. Moreover, it has shown that detrimental over-polarization effects between the quantum system and the classical polarizable embedding start to play a role only with very large basis sets, including many diffuse functions (e.g., aug-cc-pVQZ and larger). This result is in principle dependent on the system chosen. However, the combination of oppositely charged QM molecule and classical embedding tested here should represent a challenging case: the results obtained for both excited-state geometry optimizations and fluorescence energies clearly indicate that even rather extended basis sets can be used in combination with polarizable QM/MM. Of course these findings have to be confirmed by further studies on different molecular probes and different types of environments. However, it is clear that atomistic models able to include polarization represent a very effective strategy to study photoinduced processes in complex biosystems.

■ ASSOCIATED CONTENT

Supporting Information

The Supporting Information is available free of charge on the ACS Publications website at DOI: 10.1021/acs.jctc.7b00475.

Cartesian coordinates of optimized ground and excited state of free and intercalated DAPI at the CAM-B3LYP level; list of relevant geometrical parameters optimized with different functionals; charge distribution analysis; absorption and emission energies and transition dipole moments (PDF)

Jmol files (ZIP)

■ AUTHOR INFORMATION

Corresponding Author

*E-mail: benedetta.mennucci@unipi.it.

ORCID

Benedetta Mennucci: 0000-0002-4394-0129

Funding

M.M. gratefully acknowledges financial support from the EU Horizon 2020 research and innovation program under the Marie Skłodowska-Curie grant agreement No. 642294.

Notes

The authors declare no competing financial interest.

■ REFERENCES

(1) Tomasi, J.; Persico, M. Molecular Interactions in Solution: an Overview of Methods Based on Continuous Distributions of the Solvent. *Chem. Rev.* **1994**, *94*, 2027−2094.

(2) Cramer, C. J.; Truhlar, D. G. Implicit Solvation Models: Equilibria, Structure, Spectra, and Dynamics. *Chem. Rev.* **1999**, *99*, 2161−2200.

(3) Tomasi, J.; Mennucci, B.; Cammi, R. Quantum Mechanical Continuum Solvation Models. *Chem. Rev.* **2005**, *105*, 2999−3094.

(4) Gao, J. Hybrid Quantum and Molecular Mechanical Simulations: An Alternative Avenue to Solvent Effects in Organic Chemistry. *Acc. Chem. Res.* **1996**, *29*, 298−305.

(5) Lin, H.; Truhlar, D. G. QM/MM: What Have We Learned, Where Are We, and Where Do We Go from Here? *Theor. Chem. Acc.* **2007**, *117*, 185−199.

(6) Senn, H. M.; Thiel, W. QM/MM Methods for Biomolecular Systems. *Angew. Chem., Int. Ed.* **2009**, *48*, 1198−1229.

(7) Mennucci, B. Modeling Absorption and Fluorescence Solvatochromism with QM/Classical Approaches. *Int. J. Quantum Chem.* **2015**, *115*, 1202−1208.

(8) List, N. H.; Olsen, J. M. H.; Kongsted, J. Excited States in Large Molecular Systems through Polarizable Embedding. *Phys. Chem. Chem. Phys.* **2016**, *18*, 20234−20250.

(9) Scalmani, G.; Frisch, M. J.; Mennucci, B.; Tomasi, J.; Cammi, R.; Barone, V. Geometries and Properties of Excited States in the Gas Phase and in Solution: Theory and Application of a Time-Dependent Density Functional Theory Polarizable Continuum Model. *J. Chem. Phys.* **2006**, *124*, 094107.

(10) Bjorgaard, J. A.; Velizhanin, K. A.; Tretiak, S. Solvent Effects in Time-Dependent Self-Consistent Field Methods. II. Variational Formulations and Analytical Gradients. *J. Chem. Phys.* **2015**, *143*, 054305−10.

(11) Gordon, M. S.; Freitag, M. A.; Bandyopadhyay, P.; Jensen, J. H.; Kairys, V.; Stevens, W. J. The Effective Fragment Potential Method: A QM-Based MM Approach to Modeling Environmental Effects in Chemistry. *J. Phys. Chem. A* **2001**, *105*, 293−307.

(12) Minezawa, N.; De Silva, N.; Zahariev, F.; Gordon, M. S. Implementation of the Analytic Energy Gradient for the Combined Time-Dependent Density Functional Theory/Effective Fragment Potential Method: Application to Excited-State Molecular Dynamics Simulations. *J. Chem. Phys.* **2011**, *134*, 054111.

(13) Cammi, R.; Corni, S.; Mennucci, B.; Tomasi, J. Electronic Excitation Energies of Molecules in Solution: State Specific and Linear Response Methods for Nonequilibrium Continuum Solvation Models. *J. Chem. Phys.* **2005**, *122*, 104513.

(14) Corni, S.; Cammi, R.; Mennucci, B.; Tomasi, J. Electronic Excitation Energies of Molecules in Solution within Continuum Solvation Models: Investigating the Discrepancy between State-Specific and Linear-Response Methods. *J. Chem. Phys.* **2005**, *123*, 134512.

(15) Lunkenheimer, B.; Köhn, A. Solvent Effects on Electronically Excited States Using the Conductor-Like Screening Model and the Second-Order Correlated Method ADC(2). *J. Chem. Theory Comput.* **2013**, *9*, 977−994.

(16) Schwabe, T. General Theory for Environmental Effects on (Vertical) Electronic Excitation Energies. *J. Chem. Phys.* **2016**, *145*, 154105.

(17) Caricato, M.; Mennucci, B.; Tomasi, J.; Ingrosso, F.; Cammi, R.; Corni, S.; Scalmani, G. Formation and Relaxation of Excited States in Solution: A New Time Dependent Polarizable Continuum Model

Based on Time Dependent Density Functional Theory. *J. Chem. Phys.* **2006**, *124*, 124520.
(18) Improta, R.; Barone, V.; Scalmani, G.; Frisch, M. J. A State-Specific Polarizable Continuum Model Time Dependent Density Functional Theory Method for Excited State Calculations in Solution. *J. Chem. Phys.* **2006**, *125*, 054103.
(19) Marenich, A. V.; Cramer, C. J.; Truhlar, D. G.; Guido, C. A.; Mennucci, B.; Scalmani, G.; Frisch, M. J. Practical Computation of Electronic Excitation in Solution: Vertical Excitation Model. *Chem. Sci.* **2011**, *2*, 2143−2161.
(20) Guareschi, R.; Valsson, O.; Curutchet, C.; Mennucci, B.; Filippi, C. Electrostatic versus Resonance Interactions in Photoreceptor Proteins: The Case of Rhodopsin. *J. Phys. Chem. Lett.* **2016**, *7*, 4547−4553.
(21) Loco, D.; Polack, É.; Caprasecca, S.; Lagardère, L.; Lipparini, F.; Piquemal, J.-P.; Mennucci, B. A QM/MM Approach Using the AMOEBA Polarizable Embedding: From Ground State Energies to Electronic Excitations. *J. Chem. Theory Comput.* **2016**, *12*, 3654−3661.
(22) Chibani, S.; Laurent, A. D.; Blondel, A.; Mennucci, B.; Jacquemin, D. Excited-State Geometries of Solvated Molecules: Going Beyond the Linear-Response Polarizable Continuum Model. *J. Chem. Theory Comput.* **2014**, *10*, 1848−1851.
(23) Mennucci, B.; Scalmani, G.; Jacquemin, D. Excited-State Vibrations of Solvated Molecules: Going Beyond the Linear-Response Polarizable Continuum Model. *J. Chem. Theory Comput.* **2015**, *11*, 847−850.
(24) Curutchet, C.; Muñoz-Losa, A.; Monti, S.; Kongsted, J.; Scholes, G. D.; Mennucci, B. Electronic Energy Transfer in Condensed Phase Studied by a Polarizable QM/MM Model. *J. Chem. Theory Comput.* **2009**, *5*, 1838−1848.
(25) Caprasecca, S.; Jurinovich, S.; Viani, L.; Curutchet, C.; Mennucci, B. Geometry Optimization in Polarizable QM/MM Models: The Induced Dipole Formulation. *J. Chem. Theory Comput.* **2014**, *10*, 1588−1598.
(26) Chung, L. W.; Sameera, W. M. C.; Ramozzi, R.; Page, A. J.; Hatanaka, M.; Petrova, G. P.; Harris, T. V.; Li, X.; Ke, Z.; Liu, F.; Li, H.-B.; Ding, L.; Morokuma, K. The ONIOM Method and Its Applications. *Chem. Rev.* **2015**, *115*, 5678−5796.
(27) Thole, B. T. Molecular Polarizabilities Calculated with a Modified Dipole Interaction. *Chem. Phys.* **1981**, *59*, 341.
(28) van Duijnen, P. T.; Swart, M. Molecular and Atomic Polarizabilities: Thole's Model Revisited. *J. Phys. Chem. A* **1998**, *102*, 2399.
(29) Wang, J.; Cieplak, P.; Li, J.; Wang, J.; Cai, Q.; Hsieh, M.; Lei, H.; Luo, R.; Duan, Y. *J. Phys. Chem. B* **2011**, *115*, 3100.
(30) Sala, J.; Guàrdia, E.; Masia, M. The Polarizable Point Dipoles Method with Electrostatic Damping: Implementation on a Model System. *J. Chem. Phys.* **2010**, *133*, 234101.
(31) Casida, M. E.; Jamorski, C.; Casida, K. C.; Salahub, D. R. Molecular Excitation Energies to High-Lying Bound States from Time-Dependent Density-Functional Response Theory: Characterization and Correction of the Time-Dependent Local Density Approximation Ionization Threshold. *J. Chem. Phys.* **1998**, *108*, 4439−4449.
(32) Pulay, P. Ab Initio Calculation of Force Constants and Equilibrium Geometries in Polyatomic Molecules. *Mol. Phys.* **1969**, *17*, 197−204.
(33) Furche, F.; Ahlrichs, R. Adiabatic Time-Dependent Density Functional Methods for Excited State Properties. *J. Chem. Phys.* **2002**, *117*, 7433−15.
(34) Carnimeo, I.; Cappelli, C.; Barone, V. Analytical gradients for MP2, double hybrid functionals, and TD-DFT with polarizable embedding described by fluctuating charges. *J. Comput. Chem.* **2015**, *36*, 2271−2290.
(35) Handy, N. C.; Schaefer, H. F., III On the evaluation of analytic energy derivatives for correlated wave functions. *J. Chem. Phys.* **1984**, *81*, 5031−5033.
(36) Frisch, M. J.; Trucks, G. W.; Schlegel, H. B.; Scuseria, G. E.; Robb, M. A.; Cheeseman, J. R.; Scalmani, G.; Barone, V.; Mennucci, B.; Petersson, G. A.; Nakatsuji, H.; Caricato, M.; Li, X.; Hratchian, H. P.; Izmaylov, A. F.; Bloino, J.; Zheng, G.; Sonnenberg, J. L.; Hada, M.; Ehara, M.; Toyota, K.; Fukuda, R.; Hasegawa, J.; Ishida, M.; Nakajima, T.; Honda, Y.; Kitao, O.; Nakai, H.; Vreven, T.; Montgomery, J. A., Jr.; Peralta, J. E.; Ogliaro, F.; Bearpark, M.; Heyd, J. J.; Brothers, E.; Kudin, K. N.; Staroverov, V. N.; Kobayashi, R.; Normand, J.; Raghavachari, K.; Rendell, A.; Burant, J. C.; Iyengar, S. S.; Tomasi, J.; Cossi, M.; Rega, N.; Millam, J. M.; Klene, M.; Knox, J. E.; Cross, J. B.; Bakken, V.; Adamo, C.; Jaramillo, J.; Gomperts, R.; Stratmann, R. E.; Yazyev, O.; Austin, A. J.; Cammi, R.; Pomelli, C.; Ochterski, J. W.; Martin, R. L.; Morokuma, K.; Zakrzewski, V. G.; Voth, G. A.; Salvador, P.; Dannenberg, J. J.; Dapprich, S.; Daniels, A. D.; Farkas, O.; Foresman, J. B.; Ortiz, J. V.; Cioslowski, J.; Fox, D. J. *Gaussian 09 Revision A.1*; Gaussian, Inc.: Wallingford, CT, 2009. www.gaussian.com (accessed July 20, 2017).
(37) Kapuscinski, J. DAPI: A DNA-Specific Fluorescent Probe. *Biotech. Histochem.* **1995**, *70*, 220−233.
(38) Wilson, W. D.; Tanious, F. A.; Barton, H. J.; Jones, R. L.; Strekowski, L.; Boykin, D. W. Binding of 4′,6-Diamidino-2-Phenylindole (DAPI) to GC and Mixed Sequences in DNA: Intercalation of a Classical Groove-Binding Molecule. *J. Am. Chem. Soc.* **1989**, *111*, 5008−5010.
(39) Trotta, E.; D'Ambrosio, E.; Ravagnan, G.; Paci, M. Evidence for DAPI Intercalation in CG Sites of DNA Oligomer [d-(CGACGTCG)]2: A 1H NMR Study. *Nucleic Acids Res.* **1995**, *23*, 1333−1340.
(40) Biancardi, A.; Biver, T.; Secco, F.; Mennucci, B. An Investigation of the Photophysical Properties of Minor Groove Bound and Intercalated DAPI Through Quantum-Mechanical and Spectroscopic Tools. *Phys. Chem. Chem. Phys.* **2013**, *15*, 4596−4603.
(41) Wang, J.; Cieplak, P.; Li, J.; Hou, T.; Luo, R.; Duan, Y. Development of Polarizable Models for Molecular Mechanical Calculations I: Parameterization of Atomic Polarizability. *J. Phys. Chem. B* **2011**, *115*, 3091−9.
(42) Wang, J.; Cieplak, P.; Li, J.; Wang, J.; Cai, Q.; Hsieh, M.; Lei, H.; Luo, R.; Duan, Y. Development of Polarizable Models for Molecular Mechanical Calculations II: Induced Dipole Models Significantly Improve Accuracy of Intermolecular Interaction Energies. *J. Phys. Chem. B* **2011**, *115*, 3100−3111.
(43) Caprasecca, S.; Curutchet, C.; Mennucci, B.; Jurinovich, S. *PolChat: A Polarisation-Consistent Charge Fitting Tool, Molecolab Tools*; University of Pisa: 2017. molecolab.dcci.unipi.it/tools/polchat (accessed July 20, 2017).
(44) Masia, M.; Probst, M.; Rey, R. On the Performance of Molecular Polarization Methods. II. Water and Carbon Tetrachloride Close to a Cation. *J. Chem. Phys.* **2005**, *123*, 164505.
(45) Masia, M.; Probst, M.; Rey, R. Polarization Damping in Halide-Water Dimers. *Chem. Phys. Lett.* **2006**, *420*, 267.

DOI: 10.1021/acs.jctc.7b00475
J. Chem. Theory Comput. 2017, 13, 3778−3786